Nucleic Acids Research, 2014 **1**
doi: 10.1093/nar/gku709

Structural and kinetic insights into binding and incorporation of *L*-nucleotide analogs by a Y-family DNA polymerase

Vineet Gaur[1], Rajan Vyas[1], Jason D. Fowler[1], Georgia Efthimiopoulos[1], Joy Y. Feng[2] and Zucai Suo[1,*]

[1]Department of Chemistry and Biochemistry, The Ohio State University, Columbus, OH 43210, USA and [2]Gilead Sciences, Inc., 333 Lakeside Drive, Foster City, CA 94044, USA

Received July 1, 2014; Revised July 17, 2014; Accepted July 18, 2014

ABSTRACT

Considering that all natural nucleotides (*D*-dNTPs) and the building blocks (*D*-dNMPs) of DNA chains possess *D*-stereochemistry, DNA polymerases and reverse transcriptases (RTs) likely possess strong *D*-stereoselectivity by preferably binding and incorporating *D*-dNTPs over unnatural *L*-dNTPs during DNA synthesis. Surprisingly, a structural basis for the discrimination against *L*-dNTPs by DNA polymerases or RTs has not been established although *L*-deoxycytidine analogs (lamivudine and emtricitabine) and *L*-thymidine (telbivudine) have been widely used as antiviral drugs for years. Here we report seven high-resolution ternary crystal structures of a prototype Y-family DNA polymerase, DNA, and *D*-dCTP, *D*-dCDP, *L*-dCDP, or the diphosphates and triphosphates of lamivudine and emtricitabine. These structures reveal that relative to *D*-dCTP, each of these *L*-nucleotides has its sugar ring rotated by 180° with an unusual O4′-*endo* sugar puckering and exhibits multiple triphosphate-binding conformations within the active site of the polymerase. Such rare binding modes significantly decrease the incorporation rates and efficiencies of these *L*-nucleotides catalyzed by the polymerase.

INTRODUCTION

Nucleotide selection by DNA polymerases has been hypothesized to be influenced by hydrogen bonds between a nascent base pair (1,2), base stacking (3), minor groove hydrogen bonds with protein residues (4,5), nucleotide desolvation (6), induced-fit protein conformational change (7–12), phosphodiester bond formation (13), positive and negative selectivity (14) and steric repulsion (15,16). In addition, shape complementarity (or geometric selection) has also been proposed to influence polymerase fidelity based on different tightness of the active sites of high- and low-fidelity DNA polymerases and different overall shapes of correct and incorrect base pairs (3). If geometric selection is stringent, it will be unlikely for a DNA polymerase to incorporate a nucleotide analog with *L*-stereochemistry (*L*-dNTP) opposite a natural templating nucleotide with *D*-stereochemistry. However, because many DNA polymerases and reverse transcriptases (RTs) can incorporate non-physiological nucleotide analogs, it might be possible for a polymerase to relax its *D*-stereoselectivity to bind and incorporate *L*-dNTPs or their analogs. This is more likely when considering that low-fidelity DNA polymerases and RTs possess flexible active sites and lack a proof-reading 3′ → 5′ exonuclease activity. The *D*-stereoselectivity of DNA polymerases and RTs has been further shown to be relaxed based on the successful development of two nucleoside reverse transcriptase inhibitors (NRTIs): lamivudine ((–)3TC; (–)-β-*L*-2′-3-dideoxy-3′-thiacytidine) and its 5-fluorinated derivative, emtricitabine ((–)FTC; (–)-β-*L*-2′-3-dideoxy-5-fluoro-3′-thiacytidine) (Figure 1), which terminate genomic replication of human immunodeficiency viruses (HIV) once converted to their triphosphate forms ((–)3TC-TP), (–)FTC-TP) and subsequently incorporated by HIV RT *in vivo*. Both (–)3TC and (–)FTC have been shown to be clinically more effective and less toxic than their enantiomeric *D*-isomers (17–21). Furthermore, (–)3TC and the third *L*-drug telbivudine (*L*-thymidine) have been used as drugs for the treatment of hepatitis B virus (HBV) infections (22,23). Like other NRTIs, the three *L*-drugs (lamivudine, emtricitabine and telbivudine) NRTIs including (–)3TC and (–)FTC also cause clinical side effects and some of them are likely associated with the inhibition of human DNA polymerases (16). Among 16 identified human DNA polymerases in the A-, B-, X- and Y-families, our recent kinetic analysis demonstrates that the DNA damage repair X-family (β and λ) and the lesion-bypass Y-family polymerases (η, κ, ι and Rev1) are more prone to inhibi-

*To whom correspondence should be addressed. Tel: +1 614 688 3706; Fax: +1 614 292 6773; Email: suo.3@osu.edu

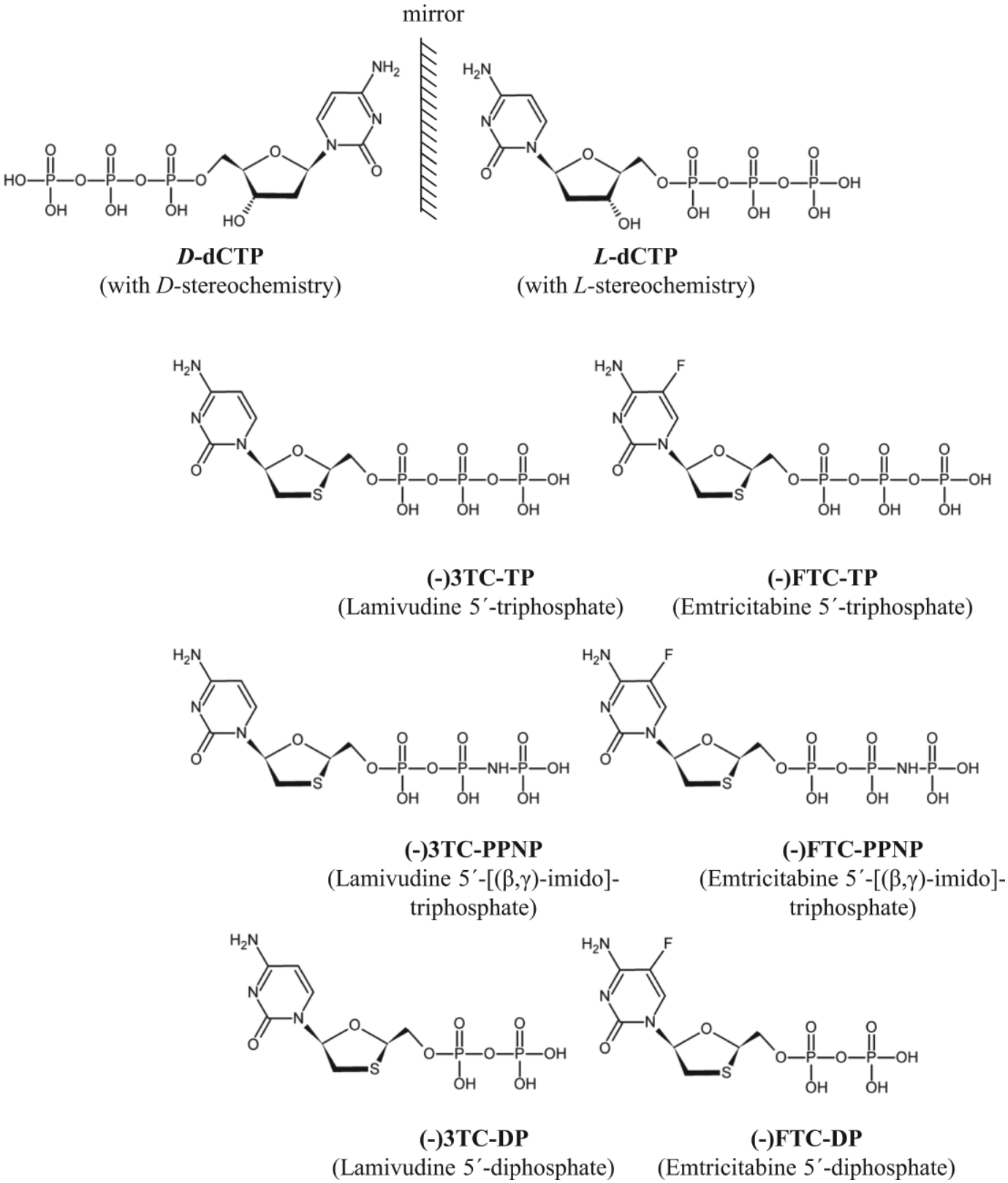

Figure 1. Chemical structures of *D*-dCTP and its *L*-analogs. The mirror emphasizes the mirror image relationship of enantiomers *D*-dCTP and *L*-dCTP.

tion by the triphosphates of the *L*-drugs than the A- and B-family, replicative polymerases (24).

To understand the molecular basis of stereoselectivity presented by a polymerase to *L*-nucleotides, we co-crystallized and solved seven ternary structures of *Sulfolobus solfataricus* DNA polymerase IV (Dpo4), a model Y-family enzyme, DNA, and either *D*-dCTP, *D*-dCDP, *L*-dCDP, the (β,γ-imido)-triphosphate derivatives ((–)3TC-PPNP) and (–)FTC-PPNP) or the diphosphates ((–)3TC-DP), (–)FTC-DP) of (–)3TC and (–)FTC (Figure 1). Since (–)3TC-TP and (–)FTC-TP were hydrolyzed to their diphosphate forms in the crystals, their non-hydrolyzable forms (–)3TC-PPNP and (–)FTC-PPNP were also included as incoming nucleotides. Notably, Dpo4 is in the same DinB subfamily as human DNA polymerase κ and has similar *in vitro* lesion-bypass activities as human DNA polymerase η (25). Therefore, our studies can provide insight into how these NRTIs may interact with human Y-family DNA polymerases besides HIV-1 RT. Our ternary structures illustrate how an *L*-nucleotide and its NRTI analogs are bound within the active site of Dpo4 prior to catalysis and explain why our pre-steady-state kinetic analysis demonstrates that Dpo4 incorporates *D*-dCTP, *L*-dCTP, (–)3TC-TP and (–)FTC-TP with dramatically different incorporation rates and efficiencies.

MATERIALS AND METHODS

Preparation of protein and DNA

Dpo4 was expressed and purified as described previously (26). DNA oligonucleotides were synthesized by Integrated DNA Technologies and purified using denaturing polyacrylamide gel electrophoresis. The regular template 18-mer (5′-TTCAGGAGTCCTGTAGCC-3′) and primer 13-mer (5′-GGCTACAGGACTC-3′) strands were annealed to form a DNA substrate 13/18-mer as described previously (26,27). For *L*-dCTP crystallization, the 3′-ddC-terminated 13-mer was used since we failed to obtain crystals using the regular 13-mer primer.

Measurement of pre-steady-state kinetic parameters for nucleotide incorporation

A pre-incubated solution of Dpo4 (240 nM) and [^{32}P]-labeled 13/18-mer (30 nM) was rapidly mixed with varying concentrations of dNTP at 37°C in buffer R (50 mM N-(2-Hydroxyethyl)piperazine-N'-(2-ethanesulfonic acid) (HEPES), pH 7.5, 5 mM $MgCl_2$, 50 mM NaCl, 0.1 mM Ethylenediaminetetraacetic acid (EDTA), 5 mM Dithiothreitol (DTT), 10% glycerol, and 0.1 mg/ml Bovine serum albumin (BSA)) in a rapid chemical quench flow apparatus (KinTek). After various times, the reaction was terminated with 0.37 M EDTA and analyzed by sequencing gel electrophoresis. Each time course of product formation was fit to a single-exponential equation, $[\text{product}] = A[1 - \exp(-k_{obs}t)]$, to yield an observed rate of nucleotide incorporation (k_{obs}) and a reaction amplitude (A). The observed rates were then plotted against dNTP concentrations and the plot was fit to a hyperbolic equation, $k_{obs} = k_p[\text{dNTP}]/([\text{dNTP}] + K_d)$, to yield an equilibrium dissociation constant (K_d) and a maximum incorporation rate (k_p).

Crystallization and structure determination

Purified Dpo4 was concentrated to 18 mg/ml and then mixed with the 13/18-mer at a molar ratio of 1:1.2 to form a binary complex in a buffer of 10 mM HEPES (pH 7.0), 5 mM $CaCl_2$, 0.5 mM DTT and 10 mM NaCl. A ternary complex was subsequently formed with the addition of 1 mM *D*-dCTP or its *L*-analogs: *L*-dCTP, (–)3TC-TP, (–)3TC-PPNP, (–)FTC-TP and (–)FTC-PPNP. Notably, non-catalytic metal ions Ca(II), rather than catalytic metal ions Mg(II), have been used regularly to trap incoming nucleotides in pre-insertion ternary complexes with Dpo4 (28–31) and other DNA polymerases (32–35). (–)3TC-TP and (–)FTC-TP were synthesized and purified by Gilead Sciences with >95% purity (HPLC). *L*-dCTP, (–)3TC-PPNP and (–)FTC-PPNP were synthesized and purified by Jena Bioscience with >95% purity (HPLC). Crystals were obtained using the hanging drop vapor diffusion method when each Dpo4 ternary complex mixture was equilibrated against a reservoir buffer composed of 12–16% PEG3350, 100 mM $Ca(Ac)_2$ and 2.5% glycerol as precipitant in 0.1 M HEPES (pH 7.0). Using 25% PEG3350 and 15% ethylene glycol in mother liquor, crystals were flash frozen in liquid nitrogen. X-ray diffraction data were collected using LRL-CAT beamline facilities at Advance Photon Source (APS), Argonne National Laboratory. X-ray diffraction data was processed using MOSFLM (36). MOLREP (37) was used for molecular replacement using PDB: 1JX4 as model (38). Structural refinement was carried out using CNS (39) and REFMAC5 (40). COOT (41) was used for visualization and model building. Quality of the models was assessed using PROCHECK (42). The torsion angles of *D*-dCTP and its *L*-analogs were calculated using PROSIT (43). Figures were created using PYMOL (44).

RESULTS AND DISCUSSION

Incorporation of *D*-dCTP and its *L*-analogs catalyzed by Dpo4

DNA polymerases catalyze phosphodiester bond formation through *in-line* nucleophilic attack of the α-phosphate of an incoming natural *D*-dNTP by a primer 3′-OH during primer elongation (Supplementary Figure S1). If the stereochemistry of the nucleotide is altered from *D* to *L*, it likely adversely influences nucleotide binding and incorporation. Consistently, our pre-steady-state kinetic analysis exploring the potential roles of various human DNA polymerases on the clinical toxicities of NRTIs demonstrates that both (–)3TC-TP and (–)FTC-TP are incorporated with maximum rates (k_p) several orders of magnitude lower than *D*-dCTP (24). Consequently, these human enzymes incorporate *D*-dCTP over (–)3TC-TP and (–)FTC-TP with 40–290 000-fold higher incorporation efficiencies (k_p/K_d) (24). Unlike replicative DNA polymerases, several human X- and Y-family DNA polymerases can incorporate these *L*-NRTIs as efficiently as HIV-1 RT (24). Likewise, Dpo4, the lone lesion-bypass Y-family DNA polymerase from *S. solfataricus*, was able to incorporate *L*-

dCTP, (–)3TC-TP and (–)FTC-TP but with k_p and k_p/K_d lowered by 10^3–10^4-fold relative to those of *D*-dCTP, leading to calculated *D*-stereoselectivity of 4.4×10^4, 1.9×10^3 and 6.2×10^2, respectively (Table 1 and Supplementary Figure S2A–L). Additionally, the *L*-stereochemistry modestly affected the binding affinity ($1/K_d$) of an incoming nucleotide to the binary complex Dpo4·DNA based on the K_d values of *D*-dCTP and its three *L*-analogs. In addition, both k_p and k_p/K_d follow the order of *D*-dCTP >> (–)FTC-TP > (–)3TC-TP > *L*-dCTP (Table 1). Notably, the 5-fluorination of the base (Figure 1) makes (–)FTC-TP a better substrate than (–)3TC-TP to both Dpo4 (Table 1) and HIV-1 RT (18) while the chemical modifications on both the ribose and the base improve the k_p/K_d of (–)FTC-TP over *L*-dCTP by ~100-fold and decrease the *D*-stereoselectivity to only 620 with Dpo4 (Table 1). To establish a structural basis for the differences in the binding and incorporation kinetic parameters of these *L*-nucleotides, we performed crystallographic studies with Dpo4 in complex with DNA and *L*-nucleotides.

Overall ternary structures

After numerous attempts, we successfully crystallized ternary complexes of Dpo4, a DNA substrate 13/18-mer (see the 'Materials and Methods' section), and either *D*-dCTP, *L*-dCTP, (–)3TC-TP or (–)FTC-TP. *L*-dCTP and its two analogs were found in their diphosphate forms (Figure 2E and F and Supplementary Figure S3), which was caused by the weak phosphatase activity of Dpo4 (38). In contrast, *D*-dCTP was intact with its triphosphate moiety adopting a chair-like conformation (Figure 2A). To capture the γ-phosphate of the two *L*-NRTIs in crystal structures, non-hydrolyzable (–)3TC-PPNP and (–)FTC-PPNP (Figure 1) were synthesized and used in subsequent crystallization trials. Although slowly, both (–)3TC-PPNP and (–)FTC-PPNP can be incorporated into the 13/18-mer by Dpo4 with rates of 1.1×10^{-4} and 1.5×10^{-4} s^{-1}, respectively (Supplementary Figure S2M–O). Notably, it has been demonstrated that substitutions of β,γ-oxygen result in very low nucleotide incorporation efficiencies by DNA polymerases but have no effect on the binding conformation of these nucleotide analogs in the ternary crystal structures (45). Together, these results suggest that (–)3TC-PPNP and (–)FTC-PPNP can be good models for (–)3TC-TP and (–)FTC-TP, respectively, and the conformations of these β,γ-substituted nucleotide observed in crystal structures will closely resemble the possible conformations adopted by (–)3TC-TP and (–)FTC-TP within the active site. The crystal structures of seven Dpo4·DNA·nucleotide ternary complexes were refined to resolutions of 1.8–2.4 Å and are referred to as Dpo4-*D*-dCTP, Dpo4-*D*-dCDP, Dpo4-*L*-dCDP, Dpo4-(–)FTC-DP, Dpo4-(–)3TC-DP, Dpo4-(–)FTC-PPNP and Dpo4-(–)3TC-PPNP (Table 2, Supplementary Figures S3–S5). Notably, all seven complexes were crystallized in orthorhombic space group. Six of them were crystallized in $P2_12_12$ space group with one ternary complex molecule in an asymmetric unit while Dpo4-*L*-dCDP was crystallized in $P2_12_12_1$ space group with two ternary complex molecules (chains A and D for Dpo4) in an asymmetric unit (Supplementary Figure S3). Notably, the overall structures of Dpo4 in the seven complexes are almost identical with root-mean-square deviations between 0.37 and 0.51 Å (Supplementary Table S1, Supplementary Figures S3–S5). Thus, the overall structure of Dpo4 was not significantly affected by either the binding of a nucleotide with *L*-stereochemistry, the absence of the γ-phosphate in the incoming nucleotide, or the lack of primer 3′-OH group.

Conformations adopted by the triphosphate moiety of a polymerase-bound nucleotide

Interestingly, all three incoming *L*-nucleotides in the ternary structures were present in *anti*-conformation and formed Watson–Crick base pairs with the templating nucleotide dG (Figure 2). The triphosphate of (–)3TC-PPNP displayed a novel N-shaped conformation (Figure 2B), unlike the typically observed chair-like conformations (46) of matched *D*-dNTPs complexed with Dpo4 and undamaged DNA (Supplementary Table S2), e.g. Dpo4-*D*-dCTP (Figure 2A). In contrast, the triphosphate of (–)FTC-PPNP displayed two alternate conformations: the N-shaped conformation (Type-A, Figure 2C) and the goat tail-like conformation (46) (Type-B, Figure 2D). After several rounds of refinement with different occupancy ratios, the two conformations of (–)FTC-PPNP were best modeled with equal occupancies (Supplementary Figure S6). Although similar to (–)3TC-PPNP, the triphosphate moiety in Type-A conformation of (–)FTC-PPNP was bent slightly toward the primer 3′-terminus, allowing a water molecule to slide between Tyr12 and (–)FTC-PPNP (Figure 2C). The conformations adopted by the α- and β-phosphates in the N-shaped conformations of (–)3TC-PPNP and (–)FTC-PPNP are nearly identical to the equivalent α- and β-diphosphate moieties in Dpo4-(–)FTC-DP, Dpo4-(–)3TC-DP and Dpo4-*L*-dCDP (Figure 3 and Supplementary Figure S7) as well as the ternary structures of Dpo4·DNA·ddNDP (Supplementary Table S3), which display an *Λ*-shaped diphosphate conformation (Figure 4D). This supports our above conclusion that the (β,γ-imido)-substitution in (–)3TC-PPNP and (–)FTC-PPNP does not significantly affect the binding conformation of an incoming nucleotide. Moreover, it also indicates that either the absence of the 3′-OH of an incoming nucleotide or the mismatching of the nucleotide with a templating base significantly altered the binding conformations of the nucleotide and DNA at the active site of Dpo4. In contrast, the absence of the γ-phosphate moiety did not affect the conformation of an incoming nucleotide and the overall structure of a ternary complex, which was likely due to the positioning of the γ-phosphate moiety on the edge of the Dpo4 surface (Supplementary Figure S8A). Consistently, the nearly superimposable structures of Dpo4-*D*-dCDP and Dpo4-*D*-dCTP show that *D*-dCDP in Dpo4-*D*-dCDP is bound with an almost identical location and conformation as the counterpart of *D*-dCTP in Dpo4-*D*-dCTP (Supplementary Figure S7A).

Notably, all triphosphates of matched *D*-dNTPs in the ternary complexes with undamaged DNA and Dpo4 (Figure 2A and Supplementary Table S2) or all other DNA polymerases and RTs (Supplementary Table S4) are in a chair-like conformation. Thus, we propose this chair-like

Table 1. Kinetic parameters for nucleotide incorporation opposite the templating base dG in the 13/18-mer catalyzed by Dpo4 at 37°C

Nucleotide	k_p (s^{-1})	K_d (μM)	k_p/K_d ($\mu M^{-1}\ s^{-1}$)	*D*-stereoselectivity[a]
D-dCTP	0.70 ± 0.01	75 ± 6	9.3×10^{-3}	
L-dCTP	0.000029 ± 0.000002	138 ± 28	2.1×10^{-7}	4.4×10^{4}
(–)3TC-TP	0.00052 ± 0.00002	107 ± 11	4.8×10^{-6}	1.9×10^{3}
(–)FTC-TP	0.00084 ± 0.00005	58 ± 7	1.5×10^{-5}	6.2×10^{2}

[a] *D*-stereoselectivity = $(k_p/K_d)_{D\text{-dCTP}}/(k_p/K_d)_{L\text{-nucleotide}}$.

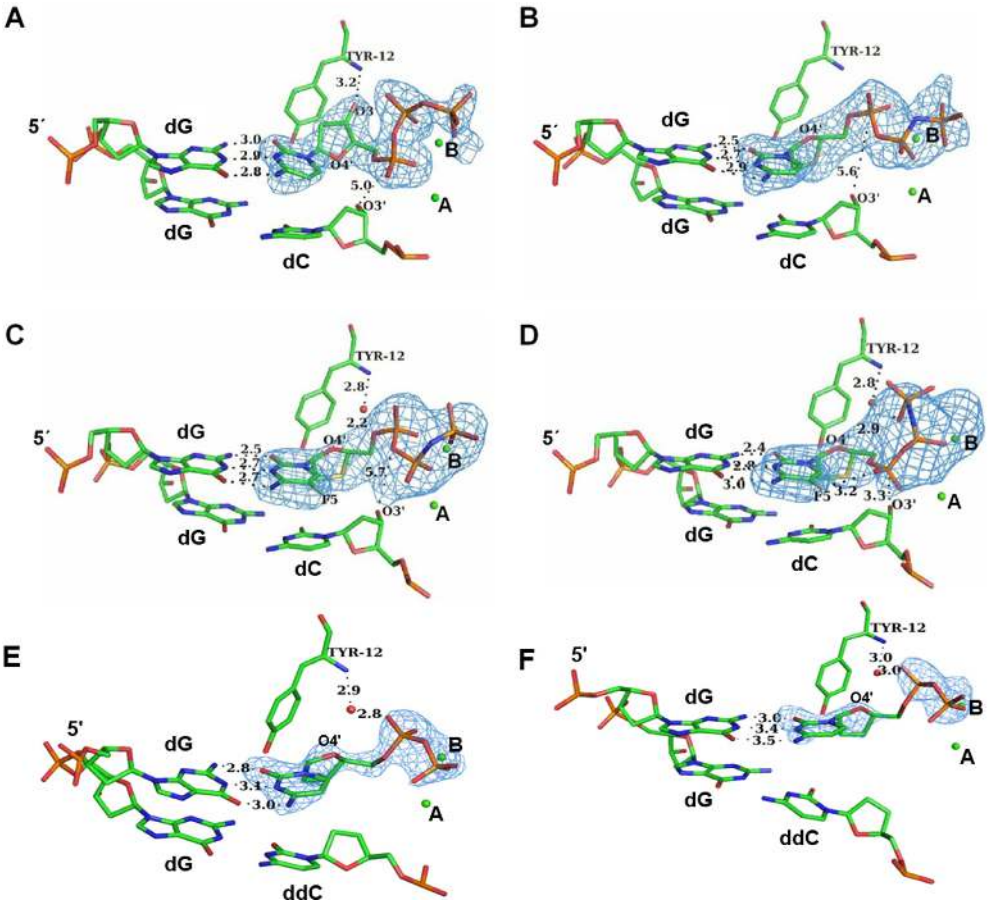

Figure 2. Interactions of *D*-dCTP or its *L*-analogs with DNA and Tyr12 within the active site of Dpo4. (**A**) *D*-dCTP (2.3 Å resolution); (**B**) (–)3TC-PPNP (2.1 Å resolution); (**C**) Type-A conformation of (–)FTC-PPNP (2.4 Å resolution); (**D**) Type-B conformation of (–)FTC-PPNP (2.4 Å resolution); (**E**) *L*-dCDP (2.4 Å resolution, chain A) and (**F**) *L*-dCDP (2.4 Å resolution, chain D). Hydrogen bonds are shown in black dashed lines and the numbers depict their lengths in angstrom. The red spheres represent water molecules. Site A and site B divalent metal ions are shown as green spheres. Only two template bases and the primer 3′-terminal base of the 13/18-mer are displayed. The $F_o - F_c$ omit maps for incoming nucleotides are shown in blue and contoured at 3σ level. The two conformations of (–)FTC-PPNP are modeled with occupancies of 0.5 each.

conformation to be a part of a productive ternary complex during catalysis. In contrast, the triphosphate groups of a mismatched *D*-dNTP and matched *D*-ddNDPs (Supplementary Table S3) as well as matched *L*-nucleotides described here (projected from Figure 2E) are in the goat tail-like and/or N-shaped conformations, which we consider to be less productive based on significantly lower k_p and k_p/K_d values of (–)3TC-TP and (–)FTC-TP than correct *D*-dCTP (Table 1). These conclusions are further supported by the interaction patterns between the two divalent metal ions and the triphosphate moiety in the three conformations (Supplementary Figure S9): the pattern in the chair-like conformation is optimized for catalysis (47). Although we failed to obtain the ternary structure of Dpo4-*L*-dCTP (see above), the Λ-shaped diphosphate binding conformation of *L*-dCDP in the Dpo4-*L*-dCDP (Figure 2E and F), which is similar to the counter parts in Dpo4-(–)FTC-DP and Dpo4-(–)3TC-DP (Figure 3B) as well as Type-A Dpo4-(–)FTC-PPNP (Figure 2C) and Dpo4-(–)3TC-PPNP (Figure 2B), indicates the triphosphate of *L*-dCTP was most likely bound in the non-productive N-shaped conformation at the active site of Dpo4. Taken together, *L*-stereochemistry altered the binding conformation of the triphosphate of an incoming nucleotide.

Table 2. Data collection and refinement statistics

	Dpo4-*D*-dCTP	Dpo4-(−)3TC-PPNP	Dpo4-(−)FTC-PPNP	Dpo4-*D*-dCDP P236A mutant	Dpo4-*L*-dCDP	Dpo4-(−)3TC-DP	Dpo4-(−)FTC-DP
Data collection[a]							
Space group	$P2_12_12$	$P2_12_12$	$P2_12_12$	$P2_12_12$	$P2_12_12_1$	$P2_12_12$	$P2_12_12$
Cell dimensions							
a, *b*, *c* (Å)	98.1, 102.3, 52.5	96.5, 102.5, 52.4	96.8, 101.9, 52.5	96.9, 102.3, 52.7	98.4, 101.9, 105.4	96.2, 102.6, 52.6	96.7, 102.4, 52.5
α, β, γ (°)	90, 90, 90	90, 90, 90	90, 90, 90	90, 90, 90	90, 90, 90	90, 90, 90	90, 90, 90
Resolution (Å)	19.9–2.3 (2.4–2.3)	19.7–2.1 (2.2–2.1)	29.2–2.4 (2.5–2.4)	30.8–1.8 (1.84–1.80)	49.22–2.40 (2.49–2.40)	19.9–1.9 (2.0–1.9)	20.0–1.9 (2.0–1.9)
R_{merge}[b]	0.127 (0.922)	0.078 (0.802)	0.075 (0.635)	0.085 (0.859)	0.093 (0.892)	0.065 (1.354)	0.096 (1.363)
$I/\sigma I$	11.7 (4.5)	13.9 (2.5)	11.9 (1.8)	15.9 (3.0)	14.6 (2.8)	16.3 (2.5)	10.0 (1.8)
Completeness (%)	97.8 (96.5)	97.3 (94.0)	98.0 (89.4)	99.7 (99.2)	99.3 (100.0)	99.7 (100.0)	98.5 (96.2)
Redundancy	10.0 (9.5)	9.3 (6.6)	5.9 (4.3)	10.5 (10.1)	10.9 (10.0)	10.8 (10.7)	9.5 (8.6)
Refinement							
Resolution (Å)	19.9–2.3	19.7–2.1	29.2–2.4	29.3–1.80	46.46–2.40	19.9–2.2	20.0–2.2
No. of reflections	21603	26998	17427	46745	39665	23444	23266
R_{work}/R_{free}[c]	0.216/0.235	0.229/0.262	0.245/0.268	0.226/.271	0.229/0.277	0.222/0.241	0.219/0.251
No. of atoms							
Protein	2744	2744	2744	2790	5504	2744	2744
DNA	597	597	597	572	1144	597	597
Nucleotide	28	27	28	23	48	23	24
Ion	3	4	3	4	5	3	3
Water	242	271	135	307	175	283	274
Average *B*-factors (Å^2)							
Protein	36.4	47.8	63.4	28.4	64.6	49.3	45.7
DNA	43.0	55.2	72.2	31.3	78.6	61.0	56.3
Nucleotide	26.7	60.0	89.7	17.7	66.9	40.6	45.5
Ion	36.5	58.1	57.2	31.6	75.1	43.8	49.1
Water	57.6	55.6	63.5	35.5	66.4	61.6	51.6
R.M.S. deviations							
Bond lengths (Å)	0.015	0.010	0.012	0.005	0.007	0.015	0.020
Bond angles (°)	1.522	1.593	1.528	1.100	1.237	1.818	1.762

[a]Highest resolution shell is shown in parenthesis.
[b]$R_{merge} = \sum|I - <I>|/\sum I$, where I is the integrated intensity of each reflection.
[c]R value $= \sum||F_o| - |F_c||/\sum|F_o|$, where F_o and F_c are observed and calculated structure factor amplitudes.

Effect of the *L*-stereochemistry on the conformation of the sugar moiety of an incoming nucleotide

Constraints, arising from *L*-stereochemistry and Watson–Crick base pairing, led to the rotation of the sugar rings of three *L*-nucleotides by 180°, with respect to the deoxyribose of *D*-dCTP at the active site of Dpo4 (Figure 2). Consequently, the O4′ atom in each of the three *L*-nucleotides was positioned away from the primer 3′-terminus. Contrary to previously observed C3′-*endo* (29,46,48) or C2′-*endo* (38,46) sugar puckers in incoming natural *D*-dNTPs, the sugar rings of these *L*-nucleotides were found in a unique O4′-*endo* conformation (Figure 3A). Consequently, in Dpo4-(–)FTC-PPNP, Dpo4-(–)3TC-PPNP and Dpo4-*L*-dCDP, the carbon and sulfur atoms of the sugar ring formed a plane, facilitating efficient stacking interactions with the aromatic side chain of Tyr12 (Figure 3), a residue conserved among all Y-family DNA polymerases and RTs (49). Moreover, the O4′-*endo* sugar puckering, which is not the only preferred conformation for the oxathiolane ring (50), was enforced by the side chain of Tyr12 so as to avoid steric clash with the O4′ atom.

Impact of the *L*-stereochemistry of an incoming nucleotide on its binding affinity, incorporation rate and incorporation efficiency

Figure 2 indicates that *L*-dCTP and its two analogs, like *D*-dCTP, formed Watson–Crick base pairing with the templating base dG and interacted with the active site residues. Hence, the *L*-stereochemistry only modestly affected nucleotide binding affinity to Dpo4·DNA (Table 1). The 2-fold weaker binding affinity of *L*-dCTP relative to *D*-dCTP was somewhat derived from three longer Watson–Crick hydrogen bonds in *L*-dCDP:dG (average 3.0–3.3 Å) than in *D*-dCTP:dG (average 2.9 Å) (Figure 2). Due to the 180° flipping of the sugar ring (Figure 2), the 3′-OH groups of an *L*-nucleotide and the primer 3′-terminus faced each other

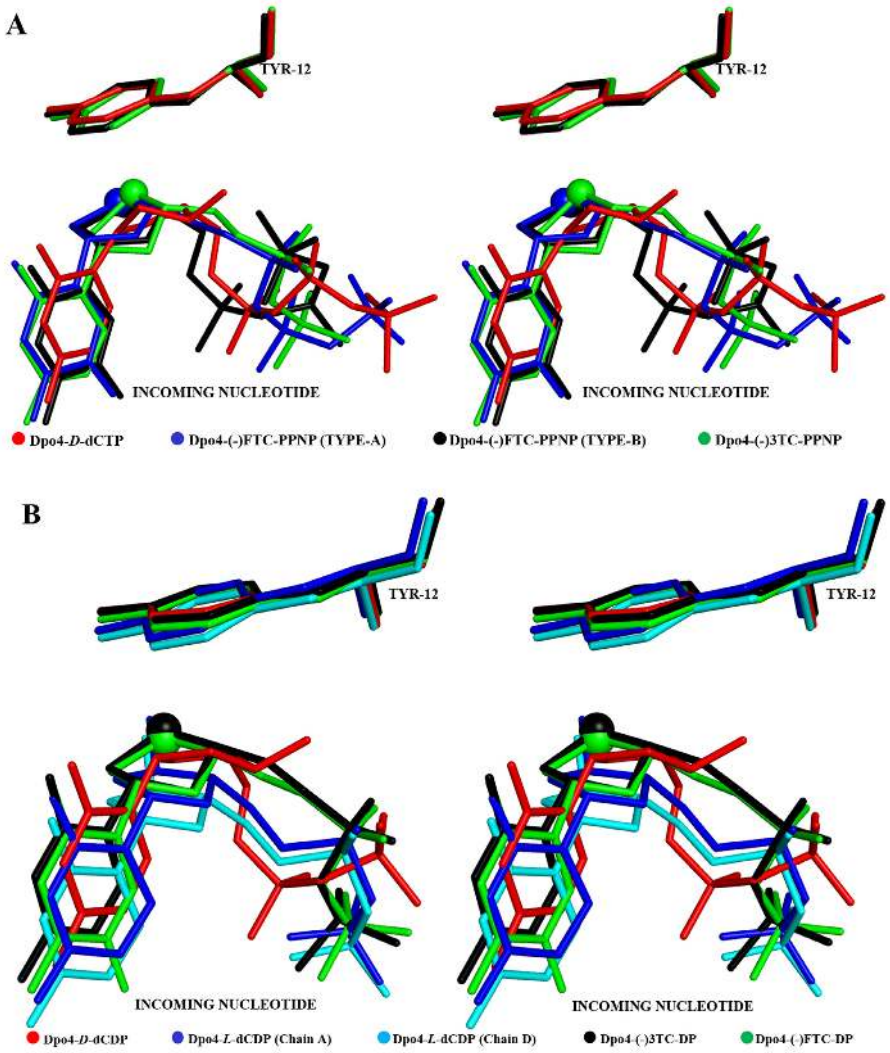

Figure 3. Difference in the stacking interactions of Tyr12 of Dpo4 with various incoming nucleotides. (**A**) Superimpositions of incoming *D*-dCTP, (–)3TC-PPNP, and Type-A and Type-B conformations of (–)FTC-PPNP in stereoview. Sulfur atoms at the 3′ positions in sugar rings are shown as spheres and (**B**) superposition incoming *D*-dCDP, *L*-dCDP (chains A and D), (–)3TCDP and (–)FTCDP in stereoview.

and could sterically clash. This steric hindrance was another potential factor contributing to lower binding affinity of *L*-dCTP than *D*-dCTP. It may be the reason why we failed to crystalize the ternary complex of Dpo4, *L*-dCTP and a normal DNA substrate containing a 3′-OH group in the primer. Such steric hindrance can be relieved by removing either of the 3′-OH groups. This is one of the reasons why both (–)3TC and (–)FTC are designed to lack the 3′-OH group. Consequently, both (–)3TC-TP and (–)FTC-TP have higher binding affinities to Dpo4·DNA than *L*-dCTP (Table 1). In addition, the affinity difference was also contributed by the slightly stronger stacking interaction between the side chain of Tyr12 and the sugar ring after the substitution of C3′ atom in *L*-dCTP with an electron-richer sulfur atom in both (–)3TC-TP and (–)FTC-TP, and by shorter Watson–Crick hydrogen bonds in (–)3TC-PPNP (or (–)FTC-PPNP):dG (average 2.6–2.7 Å) than in *L*-dCDP:dG (average 3.0–3.3 Å) (Figure 2). Interestingly, there were hydrogen bonding interaction between Tyr12 and the O5′ atom (Figure 2C) or γ-phosphate (Figure 2D) of (–)FTC-PPNP through a water bridge. However, the corresponding interaction was not observed with (–)3TC-PPNP (Figure 2B) and likely accounted for its lower binding affinity than (–)FTC-TP (Table 1).

After being bound by a polymerase, the incoming nucleotide will be efficiently incorporated into DNA if its α-phosphate moiety and the primer 3′-OH group are within a short distance and precise orientations prior to phosphodiester bond formation. Thus, a conformational rearrangement of both substrates and active site residues occurs in order to optimize the positioning of the reactive groups (51). Since *D*-dCTP was incorporated with a much higher reaction rate than its *L*-analogs (Table 1), we hypothesize that the active site structure (Figure 2A) is close to optimal for catalysis and any alteration of the structure will adversely affect nucleotide incorporation. Although unavailable, the overall structure of Dpo4-*L*-dCTP are likely similar to and can be modeled by Dpo4-*L*-dCDP (Figure 2E and F) (see above). Superimposition of the structures of Dpo4-*L*-

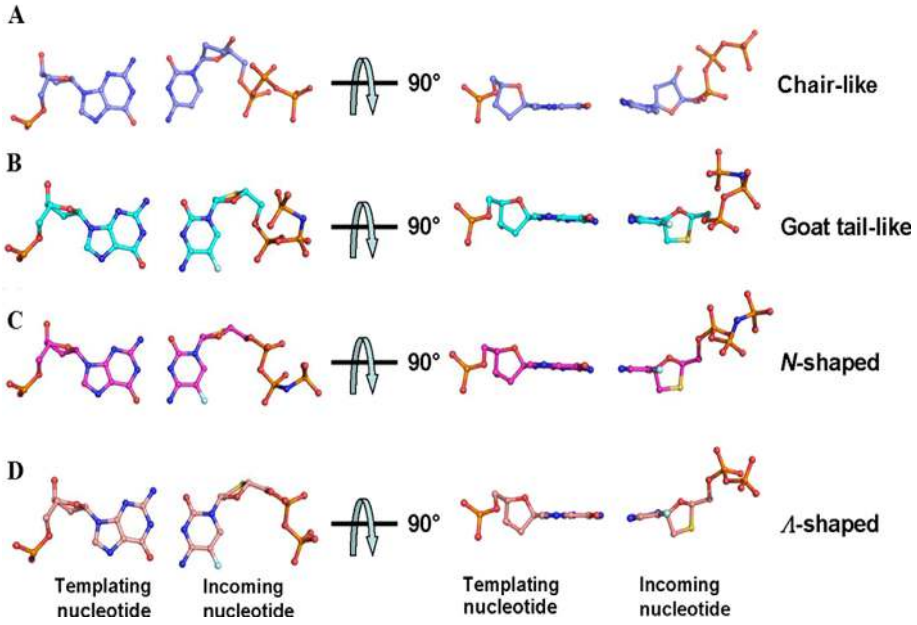

Figure 4. Conformations adopted by the triphosphate or diphosphate of an incoming nucleotide within the active site of Dpo4. (**A**) Chair-like conformation shown by *D*-dCTP; (**B**) goat tail-like conformation as shown by Type-B conformation of (–)FTC-PPNP; (**C**) N-shaped conformation as shown by (–)3TC-PPNP and Type-A conformation of (–)FTC-PPNP and (**D**) *Λ*-shaped conformation as shown by *L*-dCDP, (–)FTC-DP and (–)3TC-DP.

dCDP (Figure 2E) and Dpo4-*D*-dCTP (Figure 2A) demonstrates that besides the binding conformations of the sugar ring and the triphosphate of the incoming nucleotide (see above), the *L*-stereochemistry also dramatically altered the side-chain conformations of residues Tyr10, Thr45, Tyr48, Arg51, Glu106 and Lys152 (Supplementary Figure S8A), repositioned site A metal ion by 2.4 Å (Supplementary Figure S7C), shifted the primer/template junction base pair toward the roof of the active site (∼3.1 Å for the position of the O4′ atom of primer 3′-terminal nucleotide) (Supplementary Figure S7D), and caused steric clash between the 3′-OH groups of the nucleotide and the primer 3′-terminus (see above). Moreover, as seen with other ternary structures of Dpo4·DNA·matched *D*-dNTP (Supplementary Table S2), a hydrogen bond between the 3′-OH of *D*-dCTP and the main-chain amide of Tyr12 (Figure 2A) appears to limit the chair-like conformation adopted by the triphosphate moiety for catalysis. In the absence of this hydrogen bond, the phosphate moieties of *L*-dCTP and its analogs (Figure 2) as well as mismatched *D*-dNTP and matched *D*-ddNDPs (Supplementary Table S3) exhibit multiple conformations including non-productive goat tail-like and N-shaped (Figure 4). Although a productive chair-like conformation could not be fitted for *L*-dCTP, (–)FTC-PPNP and (–)3TC-PPNP in the crystal structures (Supplementary Figure S10), considering the flexible nature of the active site of Dpo4, a transient chair-like conformation adopted by these *L*-nucleotides cannot be excluded. The high flexibility of the triphosphate moiety of the *L*-dCTP and its analogs, especially dominated by its non-productive conformations, will not guide the precise positioning of the nucleotide for catalysis. Adding further difficulty, the distance between the primer 3′-terminal C3′ atom and the α-phosphate of an incoming nucleotide is significantly longer in Dpo4-*L*-dCDP (6.4 Å in Figure 2E and 8.8 Å in Figure 2F) than in Dpo4-*D*-dCTP (4.4 Å in in Figure 2A). Together, the long distance and above structural changes from canonical Dpo4-*D*-dCTP (Figure 2A) dramatically affected the *in-line* nucleophilic attack of the α-phosphate of the *L*-nucleotides by the primer 3′-OH during *L*-nucleotide incorporation (Supplementary Figure S1). Consistently, *L*-dCTP was incorporated with 10^4-fold lower k_p and k_p/K_d values than *D*-dCTP, leading to the high *D*-stereoselectivity of 4.4×10^4 (Table 1). Interestingly, the structural alteration observed in Dpo4-*L*-dCDP was somewhat reversed by removing the ribose 3′-OH group in Dpo4-(–)FTC-DP and Dpo4-(–)3TC-DP (Supplementary Figure S8B). For example, the junction base pair of the primer/template in both (–)3TC-DP and (–)FTC-DP was shifted back to a similar position as observed in Dpo4-*D*-dCTP. Such reverse changes likely contributed to 20–30-fold higher k_p and k_p/K_d values of (–)3TC-TP and (–)FTC-TP than *L*-dCTP, leading to relaxed *D*-stereoselectivity with these *L*-analogs (Table 1).

Notably, the distance between the α-phosphorus atom of an incoming nucleotide and the primer 3′-OH is significantly shorter for Type-B conformation of (–)FTC-PPNP (3.3 Å) than in Type-A conformation of (–)FTC-PPNP (5.7 Å) and (–)3TC-PPNP (5.6 Å) (Figure 2). Among Type-A and Type-B conformations, the latter is more similar to the chair-like conformation based on the orientation of the α-phosphate group (Figure 4). In addition, the interactions between residues Arg51 and Lys159 with the γ-phosphate group of (–)FTC-PPNP only existed in its Type-A conformation (Figure 5A), not in Type-B (Figure 5B). This suggests that transition of the triphosphate moiety of (–)FTC-PPNP to canonical chair-like conformation (Figure 4A) from the goat tail-like one (Figure 5B) was easier

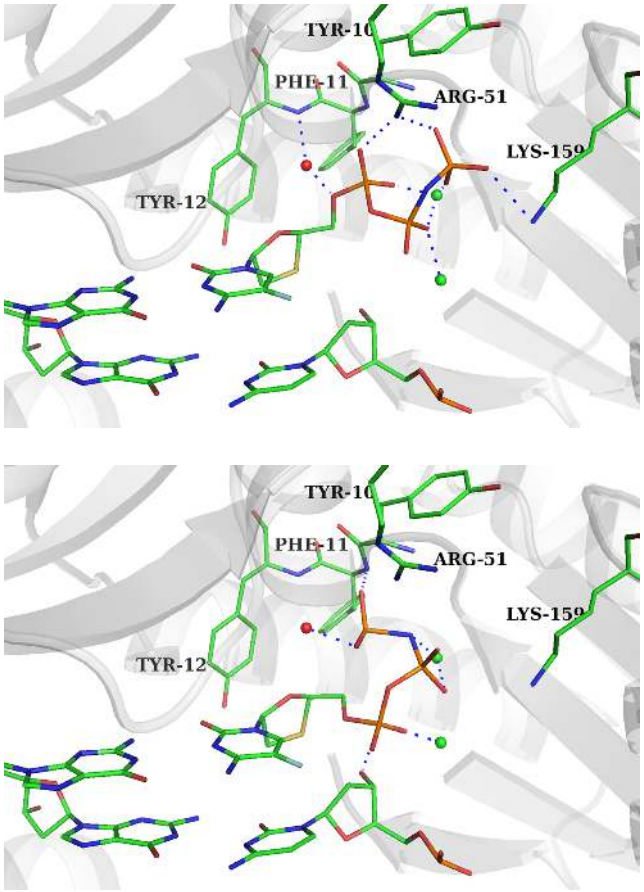

Figure 5. Interactions of an incoming (–)FTC-PPNP with the active site residues of Dpo4. (**A**) Type-A conformation and (**B**) Type-B conformation. Water molecules and active site divalent metal ions are shown in red and green spheres, respectively. Hydrogen bonds are shown as blue dashed lines.

than from the N-shaped conformation (Figure 5A). Taken together, we propose the following productive order for the triphosphate's binding conformation: chair-like >> Type-B > Type-A. Based on the similar k_p values of (–)3TC-TP and (–)FTC-TP (Table 1), (–)3TC-TP also likely adopted Type-B conformation during catalysis although this minor species was not captured during crystallization. In addition, Type-B conformation of (–)FTC-PPNP was stabilized by the presence of a weak hydrogen bond (3.2 Å) between its α-phosphate and the F5 atom of its nitrogenous base (Figure 2D). Such an interaction should not exist in the presumed Type-B conformation of (–)3TC-PPNP. The presence or absence of this intramolecular interaction altered the abundance of Type-B conformation of the *L*-analogs in solution and likely contributed to their differential incorporation efficiency with Dpo4 (Table 1) and HIV-1 RT (52).

Structural basis for varying efficiencies of *L*-nucleotide analog incorporation catalyzed by different polymerases

HIV-1 RT is a heterodimer of P66 and P51 subunits (Supplementary Figure S11A). The polymerase core domains (finger, palm and thumb) of the catalytic P66 subunit (53–55) fold into a similar right-handed structure as the corresponding domains of Dpo4 (Supplementary Figures S3–S5) and other structurally characterized DNA polymerases. Interestingly, as in Figure 2B, the sugar ring of (–)3TC-TP bound at the active site of HIV-1 RT has been predicted by a published modeling study (56) to have a 180° rotation if (–)3TC-TP possesses similar triphosphate-binding conformation and base pairing interactions with a templating base dG as *D*-dCTP. However, the *L*-nucleotides are expected not to have a highly flexible triphosphate moiety at the active site of HIV-1 RT as in Dpo4 because an additional hydrogen bond (2.4 Å) between the α-phosphate of the *D*-dNTP and the guanidinium moiety of Arg72 (Supplementary Figure S11B) stabilizes the triphosphate moiety into the chair-like conformation (53). This extra hydrogen bond will potentially restrict the conformation of the triphosphate of both (–)3TC-TP and (–)FTC-TP even in the absence of 3′-OH within the active site of HIV-1 RT (Supplementary Figure S12), not Dpo4. Consistently, HIV-1 RT incorporates (–)3TC-TP and (–)FTC-TP (average 2.3×10^{-3} μM^{-1} s^{-1}) (52) with a 300-fold higher efficiency than Dpo4 (Table 1). Similarly, our published studies have shown that human DNA polymerases ι and κ, which do not possess a corresponding Arg72 residue, incorporate (–)3TC-TP and (–)FTC-TP with considerably lower efficiency than HIV-1 RT (24). In contrast, the interaction between Arg72 of HIV-1 RT and the α-phosphate of an incoming nucleotide is also present in human DNA polymerase η (57). Consequently, the later incorporates (–)3TC-TP and (–)FTC-TP even more efficiently than the former with a DNA template (24).

Effect of *L*-stereochemistry of antiviral nucleoside analogs on drug resistance

It has been reported that clinical resistance to (–)3TC and (–)FTC treatments is associated with mutations M184V, M184I and M184T in HIV-1 RT (58–60). The model generated for the binding of *L*-dNTPs within the active site of HIV-1 RT based on the above structural studies with Dpo4 suggests that the steric hindrance, between the oxathiolane rings of (–)3TC-TP and (–)FTC-TP and the side chains of β-branched amino acid residues at position 184 (M184V, M184I and M184T) (Supplementary Figure S13), leads to the observed drug resistance. The steric hindrance is a manifestation of the 180° rotation of the sugar ring which places the relatively bulky sulfur atom of oxathiolane ring in close proximity of M184V, M184I or M184T (56). This drug resistance would be greater if the sugar ring contained a 3′-OH group. Consequently, *L*-deoxycytidine is not a good antiviral inhibitor. To reduce such drug resistance, a smaller atom, such as oxygen or carbon, can be used to substitute the sulfur atom in the oxathiolane ring of (–)3TC and (–)FTC although it will likely decrease the stacking interaction between the sugar ring and Tyr115 (Supplementary Figure S11B), leading to decreased nucleotide binding affinity.

In addition to the above three mutations, clinical data suggest that mutation K65R in HIV-1 RT also reduces (–)3TC susceptibility (60). According to our modeling studies (Supplementary Figure S13), the K65R mutant would prevent the triphosphate of (–)3TC-TP and (–)FTC-TP

from being bound in the productive chair-like conformation by sterically clashing with their γ-phosphate. However, due to the flexible nature of the side chain of arginine, the K65R mutation would only inhibit productive binding of (–)3TC-TP moderately, leading to reduced drug efficacy *in vivo*.

In summary, the ternary structures of Dpo4, DNA, and *D*-dCTP, *D*-dCDP, *L*-dCDP, (–)3TC-DP, (–)FTC-DP, (–)3TC-PPNP or (–)FTC-PPNP provide insights into how an incoming nucleotide with *L*-stereochemistry is accommodated within the active site of a Y-family DNA polymerase. The *L*-stereochemistry, sugar puckering (O4′-*endo*), and the absence of 3′-OH groups alter the binding conformation of an incoming nucleotide and the junction base pair of primer/template DNA within the active site of Dpo4 and dramatically affect nucleotide incorporation rate and efficiency. Our studies also shed light on the *D*-stereoselectivity of a DNA polymerase, and the drug efficacy and resistance of antiviral *L*-nucleoside analogs with HIV-1 RT. However, our modeling and predicted results with HIV-1 RT need to be verified by the ternary structures of HIV-1 RT, DNA or RNA, and (–)3TC-TP or (–)FTC-TP considering that Dpo4 and HIV-1 RT have very different structures and incorporate these *L*-nucleotides with 300-fold different incorporation efficiencies.

ACCESSION NUMBERS

Atomic coordinates have been deposited in the Protein Data Bank (www.rcsb.org) under accession codes: 4QW8 (Dpo4-*D*-dCTP), 4QWB (Dpo4-*D*-dCDP), 4QWE (Dpo4-(–)FTC-DP), 4QWA (Dpo4-(–)3TC-DP), 4QW9 (Dpo4-(–)FTC-PPNP), 4QWD (Dpo4-(–)3TC-PPNP) and 4QWC (Dpo4-*L*-dCDP).

SUPPLEMENTARY DATA

Supplementary Data are available at NAR Online.

ACKNOWLEDGMENTS

We are grateful for the access to beamline LRL-CAT (Lilly Research Laboratories Collaborative Access Team) at Advanced Photon Source (APS). Use of LRL-CAT facility was provided by Eli Lilly & Company. The authors are grateful for the usage of the Advanced Photon Source, an Office of Science User Facility operated for the U.S. Department of Energy (DOE) Office of Science by Argonne National Laboratory, which was supported by the U.S. DOE under Contract No. DE-AC02-06CH11357. The authors are also grateful for the usage of the LRL-CAT beamline at Sector 31 of the APS provided by Eli Lilly Company, which operates the facility.

FUNDING

National Science Foundation [MCB-0960961 to Z.S.]; Nation Institutes of Health [ES009127 to Z.S.]. Funding for open access charge: National Science Foundation [MCB-0960961].
Conflict of interest statement. None declared.

REFERENCES

1. Lee,H.R., Helquist,S.A., Kool,E.T. and Johnson,K.A. (2008) Base pair hydrogen bonds are essential for proofreading selectivity by the human mitochondrial DNA polymerase. *J. Biol. Chem.*, **283**, 14411–14416.
2. Washington,M.T., Helquist,S.A., Kool,E.T., Prakash,L. and Prakash,S. (2003) Requirement of Watson-Crick hydrogen bonding for DNA synthesis by yeast DNA polymerase eta. *Mol. Cell. Biol.*, **23**, 5107–5112.
3. Kool,E.T. (2001) Hydrogen bonding, base stacking, and steric effects in dna replication. *Annu. Rev. Biophys. Biomol. Struct.*, **30**, 1–22.
4. Pelletier,H., Sawaya,M.R., Kumar,A., Wilson,S.H. and Kraut,J. (1994) Structures of ternary complexes of rat DNA polymerase beta, a DNA template-primer, and ddCTP. *Science*, **264**, 1891–1903.
5. Bebenek,K., Beard,W.A., Darden,T.A., Li,L., Prasad,R., Luton,B.A., Gorenstein,D.G., Wilson,S.H. and Kunkel,T.A. (1997) A minor groove binding track in reverse transcriptase. *Nat. Struct. Biol.*, **4**, 194–197.
6. Petruska,J., Sowers,L.C. and Goodman,M.F. (1986) Comparison of nucleotide interactions in water, proteins, and vacuum: model for DNA polymerase fidelity. *Proc. Natl. Acad. Sci. U.S.A.*, **83**, 1559–1562.
7. Wong,I., Patel,S.S. and Johnson,K.A. (1991) An induced-fit kinetic mechanism for DNA replication fidelity: direct measurement by single-turnover kinetics. *Biochemistry*, **30**, 526–537.
8. Fiala,K.A. and Suo,Z. (2004) Mechanism of DNA polymerization catalyzed by Sulfolobus solfataricus P2 DNA polymerase IV. *Biochemistry*, **43**, 2116–2125.
9. Washington,M.T., Prakash,L. and Prakash,S. (2001) Yeast DNA polymerase eta utilizes an induced-fit mechanism of nucleotide incorporation. *Cell*, **107**, 917–927.
10. Kuchta,R.D., Mizrahi,V., Benkovic,P.A., Johnson,K.A. and Benkovic,S.J. (1987) Kinetic mechanism of DNA polymerase I (Klenow). *Biochemistry*, **26**, 8410–8417.
11. Frey,M.W., Sowers,L.C., Millar,D.P. and Benkovic,S.J. (1995) The nucleotide analog 2-aminopurine as a spectroscopic probe of nucleotide incorporation by the Klenow fragment of Escherichia coli polymerase I and bacteriophage T4 DNA polymerase. *Biochemistry*, **34**, 9185–9192.
12. Capson,T.L., Peliska,J.A., Kaboord,B.F., Frey,M.W., Lively,C., Dahlberg,M. and Benkovic,S.J. (1992) Kinetic characterization of the polymerase and exonuclease activities of the gene 43 protein of bacteriophage T4. *Biochemistry*, **31**, 10984–10994.
13. Showalter,A.K. and Tsai,M.D. (2002) A reexamination of the nucleotide incorporation fidelity of DNA polymerases. *Biochemistry*, **41**, 10571–10576.
14. Beckman,J., Kincaid,K., Hocek,M., Spratt,T., Engels,J., Cosstick,R. and Kuchta,R.D. (2007) Human DNA polymerase alpha uses a combination of positive and negative selectivity to polymerize purine dNTPs with high fidelity. *Biochemistry*, **46**, 448–460.
15. Brown,J.A. and Suo,Z. (2011) Unlocking the sugar 'steric gate' of DNA polymerases. *Biochemistry*, **50**, 1135–1142.
16. Joyce,C.M. and Benkovic,S.J. (2004) DNA polymerase fidelity: kinetics, structure, and checkpoints. *Biochemistry*, **43**, 14317–14324.
17. Feng,J.Y. and Anderson,K.S. (1999) Mechanistic studies comparing the incorporation of (+) and (–) isomers of 3TCTP by HIV-1 reverse transcriptase. *Biochemistry*, **38**, 55–63.
18. Feng,J.Y., Shi,J., Schinazi,R.F. and Anderson,K.S. (1999) Mechanistic studies show that (–)-FTC-TP is a better inhibitor of HIV-1 reverse transcriptase than 3TC-TP. *FASEB J.*, **13**, 1511–1517.
19. Gumina,G., Chong,Y., Choo,H., Song,G.Y. and Chu,C.K. (2002) L-nucleosides: antiviral activity and molecular mechanism. *Curr. Top. Med. Chem.*, **2**, 1065–1086.
20. Chang,C.N., Skalski,V., Zhou,J.H. and Cheng,Y.C. (1992) Biochemical pharmacology of (+)- and (–)-2′,3′-dideoxy-3′-thiacytidine as anti-hepatitis B virus agents. *J. Biol. Chem.*, **267**, 22414–22420.
21. Schinazi,R.F., McMillan,A., Cannon,D., Mathis,R., Lloyd,R.M., Peck,A., Sommadossi,J.P., St Clair,M., Wilson,J., Furman,P.A. *et al.* (1992) Selective inhibition of human immunodeficiency viruses by racemates and enantiomers of cis-5-fluoro-1-[2-(hydroxymethyl)-1,3-oxathiolan-5-yl]cytosine. *Antimicrob. Agents Chemother.*, **36**, 2423–2431.

22. Zemlicka,J. (2000) Enantioselectivity of the antiviral effects of nucleoside analogues. *Pharmacol. Ther.*, **85**, 251–266.
23. Brown,J.A., Pack,L.R., Fowler,J.D. and Suo,Z. (2012) Presteady state kinetic investigation of the incorporation of anti-hepatitis B nucleotide analogues catalyzed by noncanonical human DNA polymerases. *Chem. Res. Toxicol.*, **25**, 225–233.
24. Brown,J.A., Pack,L.R., Fowler,J.D. and Suo,Z. (2011) Pre-steady-state kinetic analysis of the incorporation of anti-HIV nucleotide analogs catalyzed by human X- and Y-family DNA polymerases. *Antimicrob. Agents Chemother.*, **55**, 276–283.
25. Boudsocq,F., Iwai,S., Hanaoka,F. and Woodgate,R. (2001) Sulfolobus solfataricus P2 DNA polymerase IV (Dpo4): an archaeal DinB-like DNA polymerase with lesion-bypass properties akin to eukaryotic poleta. *Nucleic Acids Res.*, **29**, 4607–4616.
26. Fiala,K.A. and Suo,Z. (2004) Pre-steady-state kinetic studies of the fidelity of Sulfolobus solfataricus P2 DNA polymerase IV. *Biochemistry*, **43**, 2106–2115.
27. Maxwell,B.A. and Suo,Z. (2012) Kinetic basis for the differing response to an oxidative lesion by a replicative and a lesion bypass DNA polymerase from Solfolobus solfataricus. *Biochemistry*, **51**, 3485–3496.
28. Irimia,A., Eoff,R.L., Pallan,P.S., Guengerich,F.P. and Egli,M. (2007) Structure and activity of Y-class DNA polymerase DPO4 from Sulfolobus solfataricus with templates containing the hydrophobic thymine analog 2,4-difluorotoluene. *J. Biol. Chem.*, **282**, 36421–36433.
29. Eoff,R.L., Irimia,A., Egli,M. and Guengerich,F.P. (2007) Sulfolobus solfataricus DNA polymerase Dpo4 is partially inhibited by "wobble" pairing between O6-methylguanine and cytosine, but accurate bypass is preferred. *J. Biol. Chem.*, **282**, 1456–1467.
30. Eoff,R.L., Irimia,A., Angel,K.C., Egli,M. and Guengerich,F.P. (2007) Hydrogen bonding of 7,8-dihydro-8-oxodeoxyguanosine with a charged residue in the little finger domain determines miscoding events in Sulfolobus solfataricus DNA polymerase Dpo4. *J. Biol. Chem.*, **282**, 19831–19843.
31. Eoff,R.L., Stafford,J.B., Szekely,J., Rizzo,C.J., Egli,M., Guengerich,F.P. and Marnett,L.J. (2009) Structural and functional analysis of Sulfolobus solfataricus Y-family DNA polymerase Dpo4-catalyzed bypass of the malondialdehyde-deoxyguanosine adduct. *Biochemistry*, **48**, 7079–7088.
32. Swan,M.K., Johnson,R.E., Prakash,L., Prakash,S. and Aggarwal,A.K. (2009) Structural basis of high-fidelity DNA synthesis by yeast DNA polymerase delta. *Nat. Struct. Mol. Biol.*, **16**, 979–986.
33. Franklin,M.C., Wang,J. and Steitz,T.A. (2001) Structure of the replicating complex of a pol alpha family DNA polymerase. *Cell*, **105**, 657–667.
34. Wing,R.A., Bailey,S. and Steitz,T.A. (2008) Insights into the replisome from the structure of a ternary complex of the DNA polymerase III alpha-subunit. *J. Mol. Biol.*, **382**, 859–869.
35. Irimia,A., Eoff,R.L., Guengerich,F.P. and Egli,M. (2009) Structural and functional elucidation of the mechanism promoting error-prone synthesis by human DNA polymerase kappa opposite the 7,8-dihydro-8-oxo-2′-deoxyguanosine adduct. *J. Biol. Chem.*, **284**, 22467–22480.
36. Battye,T.G., Kontogiannis,L., Johnson,O., Powell,H.R. and Leslie,A.G. (2011) iMOSFLM: a new graphical interface for diffraction-image processing with MOSFLM. *Acta Crystallogr. D Biol. Crystallogr.*, **67**, 271–281.
37. Vagin,A. and Teplyakov,A. (2010) Molecular replacement with MOLREP. *Acta Crystallogr. D Biol. Crystallogr.*, **66**, 22–25.
38. Ling,H., Boudsocq,F., Woodgate,R. and Yang,W. (2001) Crystal structure of a Y-family DNA polymerase in action: a mechanism for error-prone and lesion-bypass replication. *Cell*, **107**, 91–102.
39. Brunger,A.T., Adams,P.D., Clore,G.M., DeLano,W.L., Gros,P., Grosse-Kunstleve,R.W., Jiang,J.S., Kuszewski,J., Nilges,M., Pannu,N.S. *et al.* (1998) Crystallography & NMR system: a new software suite for macromolecular structure determination. *Acta Crystallogr. D Biol. Crystallogr.*, **54**, 905–921.
40. Murshudov,G.N., Skubak,P., Lebedev,A.A., Pannu,N.S., Steiner,R.A., Nicholls,R.A., Winn,M.D., Long,F. and Vagin,A.A. (2011) REFMAC5 for the refinement of macromolecular crystal structures. *Acta Crystallogr. D Biol. Crystallogr.*, **67**, 355–367.
41. Emsley,P. and Cowtan,K. (2004) Coot: model-building tools for molecular graphics. *Acta Crystallogr. D Biol. Crystallogr.*, **60**, 2126–2132.
42. Laskowski,R.A., Rullmannn,J.A., MacArthur,M.W., Kaptein,R. and Thornton,J.M. (1996) AQUA and PROCHECK-NMR: programs for checking the quality of protein structures solved by NMR. *J. Biomol. NMR*, **8**, 477–486.
43. Sun,G., Voigt,J.H., Marquez,V.E. and Nicklaus,M.C. (2005) Prosit, an online service to calculate pseudorotational parameters of nucleosides and nucleotides. *Nucleosides Nucleotides Nucleic Acids*, **24**, 1029–1032.
44. DeLano,W.L. (2002) *The PyMOL Molecular Graphics System*. DeLano Scientific, San Carlos, CA, U.S.A.
45. Sucato,C.A., Upton,T.G., Kashemirov,B.A., Batra,V.K., Martinek,V., Xiang,Y., Beard,W.A., Pedersen,L.C., Wilson,S.H., McKenna,C.E. *et al.* (2007) Modifying the beta,gamma leaving-group bridging oxygen alters nucleotide incorporation efficiency, fidelity, and the catalytic mechanism of DNA polymerase beta. *Biochemistry*, **46**, 461–471.
46. Vaisman,A., Ling,H., Woodgate,R. and Yang,W. (2005) Fidelity of Dpo4: effect of metal ions, nucleotide selection and pyrophosphorolysis. *EMBO J.*, **24**, 2957–2967.
47. Steitz,T.A. (1998) A mechanism for all polymerases. *Nature*, **391**, 231–232.
48. Wang,Y., Musser,S.K., Saleh,S., Marnett,L.J., Egli,M. and Stone,M.P. (2008) Insertion of dNTPs opposite the 1,N2-propanodeoxyguanosine adduct by Sulfolobus solfataricus P2 DNA polymerase IV. *Biochemistry*, **47**, 7322–7334.
49. Brown,J.A. and Suo,Z. (2011) Unlocking the sugar "steric gate" of DNA polymerases. *Biochemistry*, **50**, 1135–1142.
50. Sabini,E., Hazra,S., Konrad,M., Burley,S.K. and Lavie,A. (2007) Structural basis for activation of the therapeutic L-nucleoside analogs 3TC and troxacitabine by human deoxycytidine kinase. *Nucleic Acids Res.*, **35**, 186–192.
51. Xu,C., Maxwell,B.A., Brown,J.A., Zhang,L. and Suo,Z. (2009) Global conformational dynamics of a Y-family DNA polymerase during catalysis. *PLoS Biol.*, **7**, e1000225.
52. Feng,J.Y., Murakami,E., Zorca,S.M., Johnson,A.A., Johnson,K.A., Schinazi,R.F., Furman,P.A. and Anderson,K.S. (2004) Relationship between antiviral activity and host toxicity: comparison of the incorporation efficiencies of 2′,3′-dideoxy-5-fluoro-3′-thiacytidine-triphosphate analogs by human immunodeficiency virus type 1 reverse transcriptase and human mitochondrial DNA polymerase. *Antimicrob. Agents Chemother.*, **48**, 1300–1306.
53. Huang,H., Chopra,R., Verdine,G.L. and Harrison,S.C. (1998) Structure of a covalently trapped catalytic complex of HIV-1 reverse transcriptase: implications for drug resistance. *Science*, **282**, 1669–1675.
54. Jacobo-Molina,A., Ding,J., Nanni,R.G., Clark,A.D. Jr, Lu,X., Tantillo,C., Williams,R.L., Kamer,G., Ferris,A.L., Clark,P. *et al.* (1993) Crystal structure of human immunodeficiency virus type 1 reverse transcriptase complexed with double-stranded DNA at 3.0 A resolution shows bent DNA. *Proc. Natl. Acad. Sci. U.S.A.*, **90**, 6320–6324.
55. Kohlstaedt,L.A., Wang,J., Friedman,J.M., Rice,P.A. and Steitz,T.A. (1992) Crystal structure at 3.5 A resolution of HIV-1 reverse transcriptase complexed with an inhibitor. *Science*, **256**, 1783–1790.
56. Sarafianos,S.G., Das,K., Clark,A.D. Jr, Ding,J., Boyer,P.L., Hughes,S.H. and Arnold,E. (1999) Lamivudine (3TC) resistance in HIV-1 reverse transcriptase involves steric hindrance with beta-branched amino acids. *Proc. Natl. Acad. Sci. U.S.A.*, **96**, 10027–10032.
57. Biertumpfel,C., Zhao,Y., Kondo,Y., Ramon-Maiques,S., Gregory,M., Lee,J.Y., Masutani,C., Lehmann,A.R., Hanaoka,F. and Yang,W. (2010) Structure and mechanism of human DNA polymerase eta. *Nature*, **465**, 1044–1048.
58. Keulen,W., Back,N.K., van Wijk,A., Boucher,C.A. and Berkhout,B. (1997) Initial appearance of the 184Ile variant in lamivudine-treated patients is caused by the mutational bias of human immunodeficiency virus type 1 reverse transcriptase. *J. Virol.*, **71**, 3346–3350.
59. Schinazi,R.F., Lloyd,R.M. Jr, Nguyen,M.H., Cannon,D.L., McMillan,A., Ilksoy,N., Chu,C.K., Liotta,D.C., Bazmi,H.Z. and Mellors,J.W. (1993) Characterization of human immunodeficiency viruses resistant to oxathiolane-cytosine nucleosides. *Antimicrob. Agents Chemother.*, **37**, 875–881.

60. Deval,J., White,K.L., Miller,M.D., Parkin,N.T., Courcambeck,J., Halfon,P., Selmi,B., Boretto,J. and Canard,B. (2004) Mechanistic basis for reduced viral and enzymatic fitness of HIV-1 reverse transcriptase containing both K65R and M184V mutations. *J. Biol. Chem.*, **279**, 509–516.